Journal of Materials Chemistry A

PAPER

View Article Online
View Journal

Cite this: DOI: 10.1039/c6ta07359j

Core–shell nano-structured carbon composites based on tannic acid for lithium-ion batteries†

Chenbo Liao,[a] Qingkai Xu,[a] Chaolumen Wu,[a] Daling Fang,[b] Shengyang Chen,[a] Shimou Chen,*[b] Jiangshui Luo[c] and Lei Li*[ad]

Received 26th August 2016
Accepted 4th October 2016

DOI: 10.1039/c6ta07359j

www.rsc.org/MaterialsA

Core–shell nano-structured carbon composites have been used as electrode materials in lithium-ion batteries (LIBs) with increasing attention. The large volume swing during lithiation/delithiation processes and poor electronic conductivity are two key issues in the newly-proposed electrode materials, which severely limit their practical applications in LIBs. In order to solve these problems, we report a facile and versatile method to prepare core–shell nano-structured carbon composites using low cost and widely available tannic acid as the carbon source. The carbon layers with controlled thicknesses of 6–12 nm and 1–3 nm were coated on the surface of Si and TiO_2 nanoparticles, respectively. Due to the carbon layers, both the Si@C and TiO_2@C nanocomposites used as anode materials in LIBs showed excellent electrochemical performances including good cycling stability and high rate capability. We believe that this method may be applicable to various carbon-coating nanocomposites.

Introduction

Core–shell nano-structured carbon composites have attracted considerable attention due to their potential applications in optics, catalysis, solar cells, fuel cells and lithium-ion batteries.[1–3] In general, the core used as the major component is the nano-sized material with functional properties and the nano-scale carbon shell is used as a protection layer in order to (1) protect the core from outside environmental changes; (2) suppress core clustering and limit excessive particle growth; (3) restrict volume expansion and maintain structural integrity; and (4) improve, or bring new, physical or chemical properties. Due to these advantages, core–shell carbon nanocomposites have been widely used as electrode materials for lithium-ion batteries (LIBs) to overcome the disadvantages of nanomaterials and improve their general performance in LIBs. For example, Si@C, Sn@C, SnO_2@C and Co_3O_4@CNT core–shell nanocomposites used as anode materials showed excellent performance in LIBs since the carbon shell can offer an elastic buffering space for huge expansion/contraction.[4–8] In order to improve electronic conductivity and Li^+ ion diffusion, $LiFePO_4$@C (cathode material) and TiO_2@C (anode material) core–shell nanocomposites were also developed for application in LIBs.[9,10]

The carbon shell can be prepared using various methods, such as mechanical milling, hydrothermal or solvothermal synthesis, sol–gel process, and chemical vapor deposition (CVD) methods.[11–14] However, these methods also suffer from one or more disadvantages due to their complex or multiple stages, rigorous reaction conditions or unstable precursors. For example, mechanical milling could not offer enough volume expansion accommodation and protection from outside erosion. The hydrothermal or solvothermal methods usually require extreme conditions, such as high temperature and high pressure. The CVD method normally needs special expensive equipment, which increases production costs. In addition, it is still a big challenge to coat a uniform and continuous carbon layer on the surface of nanoparticles based on these abovementioned methods. Recently, Wu's group reported some new methods to synthesize a uniform and controllable carbon coating on Si or metal oxides, including SnO_2 and CoO, through hydrothermal carbonization of cheap saccharides and simple pyrolysis of polyvinylidene fluoride (PVDF) or polypyrrole (PPy) conducting polymers.[15–17]

Recently, core–shell carbon nanocomposites based on dopamine as a carbon source were synthesized.[18] However, this method is not suitable for practical applications since dopamine is too expensive. Herein, we report a simple and cheap method using a low-cost and widely-available carbon precursor, tannic acid (TA), to replace dopamine. TA is a type of plant polyphenol containing five digalloyl ester groups (see Scheme 1), which can be directly extracted from several natural plants such as tea, wood and oak. The cost of TA is much lower than that of

[a]Shanghai Electrochemical Energy Devices Research Center, School of Chemistry and Chemical Engineering, Shanghai Jiaotong University, Shanghai 200240, China. E-mail: lilei0323@sjtu.edu.cn

[b]Key Laboratory of Green Process and Engineering, Institute of Process Engineering, Chinese Academy of Sciences, Beijing 100190, China. E-mail: chenshimou@ipe.ac.cn

[c]Department of Materials Engineering, KU Leuven, Leuven 3001, Belgium

[d]Shanghai Key Laboratory of Electrical Insulation and Thermal Aging, School of Chemistry and Chemical Engineering, Shanghai Jiaotong University, Shanghai 200240, China

† Electronic supplementary information (ESI) available. See DOI: 10.1039/c6ta07359j

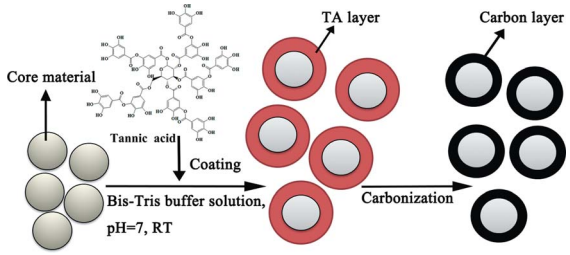

Scheme 1 Illustration of the preparation of core–shell nano-structured carbon composites using tannic acid as the carbon source.

dopamine. Similar to the polydopamine coating, the TA coating can also be formed spontaneously on virtually any surface in a bis–Tris buffer aqueous solution at room temperature.[19,20] The thickness of the TA coating can be precisely controlled from 1 to tens of nanometers.[19] The structural similarity of TA to phenolic resins prompted us to think that the TA coating should have a high carbon yield. To the best of our knowledge, however, the use of TA coating as a carbon precursor has never been reported. Considering silicon and titanium dioxide as two of the most promising anode materials for next-generation LIBs, we selected commercial Si nanoparticles (the diameter ranging from 30 to 100 nm) and commercial anatase TiO_2 nanoparticles (about 50 nm) as the core materials in our experiments. Both Si@C and TiO_2@C nanoparticles with the controlled carbon layers were prepared by TA coating followed by carbonization. The morphologies, physical and electrochemical performance including discharge specific capacity, cycling stability and rate capability of these Si@C and TiO_2@C nanocomposites used as anodes in LIBs were investigated in our experiments.

Experimental

Chemicals

Silicon nanoparticles (the diameter ranging from 30 to 100 nm) were purchased from Shanghai ST-Nano Science and Technology Co. Ltd. Anatase TiO_2 nanoparticles (about 50 nm), tannic acid (TA) and 2,2-bis(hydroxymethyl)-2,2′,2″-nitrilotriethanol (bis–Tris) were purchased from Aladdin Industrial Corporation. Battery-grade dimethyl carbonate (DMC), ethylene carbonate (EC) and $LiPF_6$ were purchased from Shenzhen Capchem Chemicals Co., Ltd., and used without further purification. Liquid electrolyte of 1 M $LiPF_6$ in a 1 : 1 (wt : wt) EC/DMC solution used in our experiments was prepared in an argon-filled glove box, in which both oxygen and water content were less than 1 ppm.

Synthesis of Si@C nanocomposites

Typically, 180 mg Si nanoparticles were dispersed in 100 mL bis–Tris buffer (100 mM buffer and 600 mM NaCl) aqueous solution of tannic acid (1.8 mg mL^{-1}, pH 7.0) at room temperature. Afterwards, the precipitates were collected by centrifugation, washed with deionized water, and then dried at 80 °C for 10 h. To carbonize the tannic acid coating, the dried powders were placed in a tube and heated to 400 °C at a rate of 1 °C min^{-1} under an Ar atmosphere and kept at this temperature for 2 h, and then heated to 800 °C with a heating rate of 5 °C min^{-1} and kept at 800 °C for 3 h. In our experiments, Si@C nanocomposites were prepared with different polymerization times: 6 h for Si@C-1, 12 h for Si@C-2 and 24 h for Si@C-3.

Synthesis of TiO_2@C nanocomposites

Typically, 200 mg anatase TiO_2 nanoparticles were dispersed in 100 mL bis–Tris buffer (100 mM buffer and 600 mM NaCl) aqueous solution of tannic acid (2.0 mg mL^{-1}, pH 7.0) at room temperature. Afterwards, the precipitates were collected by centrifugation, washed with deionized water, and then dried at 80 °C for 10 h. To carbonize the tannic acid coating, the dried powders were placed in a tube and heated to 400 °C at a rate of 1 °C min^{-1} under an Ar atmosphere and kept at this temperature for 2 h, then heated to 800 °C with a heating rate of 5 °C min^{-1} and kept at 800 °C for 3 h. In our experiments, we prepared the TiO_2@C nanocomposites with different polymerization times: 6 h for TiO_2@C-1, 12 h for TiO_2@C-2 and 24 h for TiO_2@C-3.

Characterization

Transmission electron microscopy (TEM) analysis was carried out with a JEM-2100 (JEOL Ltd., Japan) equipment operating at 200 kV. The chemical compositions of the tannic acid coated Si and TiO_2 nanocomposites were analysed by Fourier transform infrared spectroscopy (ATR-FTIR, Spectrum 100, Perkin-Elmer, Inc., USA) and X-ray photoelectron spectroscopy (XPS) (Kratos Analytical-A Shimadzu Group Company), respectively. XPS measurements were carried out by a Kratos Axis UltraDLD spectrometer using a monochromatic Al K_α radiation ($h\nu$ = 1486.6 eV). The binding energies of the samples were calibrated by taking the carbon 1s peak as a reference (284.6 eV). The weight content of carbon in the Si@C and TiO_2@C nanocomposites were determined from the weight loss curve measured under simulated air atmosphere on a TG/DTA instrument (Perkin-Elmer) with a heating rate of 10 °C min^{-1}. Electronic conductivity of TiO_2 and TiO_2@C nanocomposites was measured with the AC impedance method using an Autolab PGSTAT302 electrochemical test system (Eco Chemie, the Netherlands) at room temperature. The TiO_2 and TiO_2@C nanocomposites pellets were prepared by pressing the corresponding powders at 20 MPa. The electronic conductivity was calculated from impedance data.

In situ TEM measurement

In situ TEM observations were conducted on a JEOL JEM-2100F equipped with a Nanofactory Instruments STM-TEM holder. In order to build up the test cell, the Si@C nanocomposites were immobilized on the surfaces of multi-walled carbon nanotubes, then attached to the gold rod, which was further attached to the piezo-manipulator. On the other side, a small piece of lithium foil was attached to a sharp-tip tungsten rod as a reference and counter electrode. The electrode was affixed to the TEM holder in an Ar-filled glove box and transported to the TEM. During this transfer process, the lithium foil was exposed to air and due to

lithium being easily oxidized, the Li_2O formed on the surface of the lithium foil can act as the solid electrolyte. Inside the TEM, the metallic probes can be spatially manipulated at the nanoscale, so that with the aid of the carbon nanotubes, the Si@C nanocomposites can come into electrical contact with the Li oxide layer coating the Li electrode, forming a nanobattery inside the TEM. In this experiment, the lithiation was carried out at a negative bias in the range from −3 V to 0 V with respect to the Li metal.

Electrochemical measurements

Electrochemical properties of both Si@C and TiO_2@C nanocomposites were evaluated using CR2016 coin-type test cells. The working electrode was prepared by mixing Si@C or TiO_2@C nanocomposite, carbon black (Super P), and sodium carboxymethyl cellulose at a weight ratio of 70 : 20 : 10, and casted onto copper foil. Lithium metal was used as the counter electrode and Celgard 2400 membrane was used as the separator. The electrolyte was 1 M $LiPF_6$ in a 1 : 1 (wt : wt) EC/DMC solution. The test cells were assembled in an argon-filled glove box. The discharge–charge measurements were performed on a Land CT2001A tester (Wuhan, China) at room temperature. Electrochemical impedance spectroscopy (EIS) of the cell was observed immediately under fully charged condition. EIS measurements were accomplished by coupling the potentiostat with an Autolab frequency response analyzer locked in an amplifier and an impedance phase analyzer. A sinusoidal amplitude modulation was used over the frequency range from 0.1 Hz to 1 MHz. Cyclic voltammetry (CV) measurements of both pure nanoparticles and carbon nanocomposites were recorded on an Autolab PGSTAT302 electrochemical test system (Eco Chemie, the Netherlands) at room temperature. In our experiments, the CV measurements of both TiO_2 and TiO_2@C electrodes were tested in the potential range of 0.005–3 V at a scan rate of 0.2 mV s^{-1}, and the CV measurements of both Si and Si@C electrodes were tested in the potential range of 0.005–1.5 V at a scan rate of 0.2 mV s^{-1}.

Results and discussion

As shown in Scheme 1, the core–shell carbon nanocomposites were prepared through a two-step process. First, the TA coatings were spontaneously formed onto the surface of both Si and TiO_2 nanoparticles in a bis–Tris buffer solution of pH 7.0 in the presence of oxygen. And the color of both Si and TiO2 changed obviously after TA coating (see Fig. 1). The TA coatings on the surfaces of both Si and TiO_2 nanoparticles were confirmed by FTIR measurements (see Fig. 2). It was found that the appearance of some new peaks, considered as the characteristic peaks of TA, included at 1708 cm^{-1} (the C=O stretching vibration of the carboxylic acid group),[21] 1564 cm^{-1} (the C=C stretching vibration of the aromatic ring),[22] 1504 cm^{-1} (the C–O–H in-plane bend of the hydroxyl group),[21] 1446 cm^{-1} and 1330 cm^{-1} (the C–O stretching in the acid functionality in tannic acid),[21] 1201 cm^{-1} (the C–O stretching vibration of polyols),[23,24] 875 cm^{-1} (the C–O–C bending mode),[23,24] and 766 cm^{-1} (the C–H out-of-plane bend of the phenyl group).[23] Subsequently, the TA coatings were converted to carbon layers by carbonization in a nitrogen atmosphere at 800 °C. Through this process, the core–shell Si@C and TiO_2@C nanocomposites were obtained, as shown in Fig. 4 and 5.

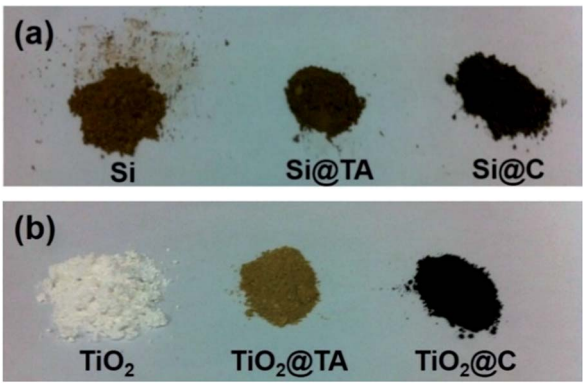

Fig. 1 Digital images of (a) Si, Si@TA and Si@C nanocomposites, and (b) TiO_2, TiO_2@TA and TiO_2@C nanocomposites.

Lee *et al.* reported that dopamine molecules had strong adhesion to surfaces, and hypothesized that both catechol (DOPA) and amine (lysine) groups on the polydopamine may bind to surfaces through covalent and/or noncovalent interactions.[25] From the chemical structure of tannic acid (see Scheme 1), we can observe that there are also some catechol groups present. In order to know the interaction between tannic acid and Si or TiO_2 nanoparticles, X-ray photoelectron spectroscopy (XPS) measurements were carried out in our experiments.

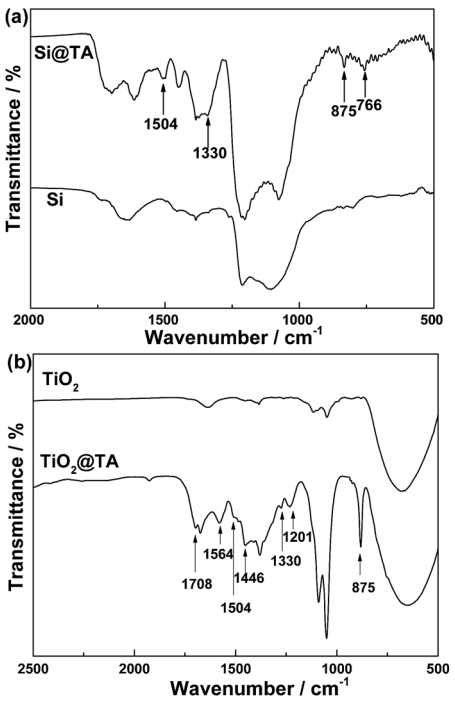

Fig. 2 FTIR spectra of (a) Si without and with the tannic acid coating, (b) TiO_2 without and with the tannic acid coating.

Fig. 3 shows O 1s spectra of pure nanoparticles (Si and TiO_2) and Si@C and TiO_2@C nanocomposites. In the spectrum of TiO_2 nanoparticles (see Fig. 3b), the main peak at the binding energy of 530.8 eV is assigned to bulk oxide (O^{2-}), and the other peak, located at 532.2 eV, is assigned to hydroxyl (OH).[26,27] The OH peak is considered to be from Ti–OH groups on the surface of the TiO_2 nanoparticles. Compared with the pristine TiO_2, there are two new peaks in the spectrum of TiO_2@TA: at 536.0 eV, assigned to the O–C, and at 531.8 eV, assigned to the O═C.[28] These results indicate the success of coating TA on the TiO_2 surface. In addition, the intensity of the Ti–OH peak was decreased compared with the pristine TiO_2, which indicates the depletion of surface Ti–OH groups. Similar results about the depletion of surface Ti–OH groups after coating have been found in the coated TiO_2 surfaces with low molecular weight catechols[29] or mPEG-DOPA polymers.[30] The possible mechanism for this may be the reaction between catechols and the Ti–OH surface, resulting in dehydration and the formation of a charge transfer complex. Similar results have been found in the spectra of Si and Si@C nanocomposites (see Fig. 3a). Compared with the pristine Si, two new peaks, at 536.4 eV and 532.0 eV, appeared in the Si@TA spectrum which are attributed to O–C and O═C groups, respectively. And the intensity of the Si–OH (at 533.8 eV assigned to OH groups) peak is also lower than that of pristine Si.

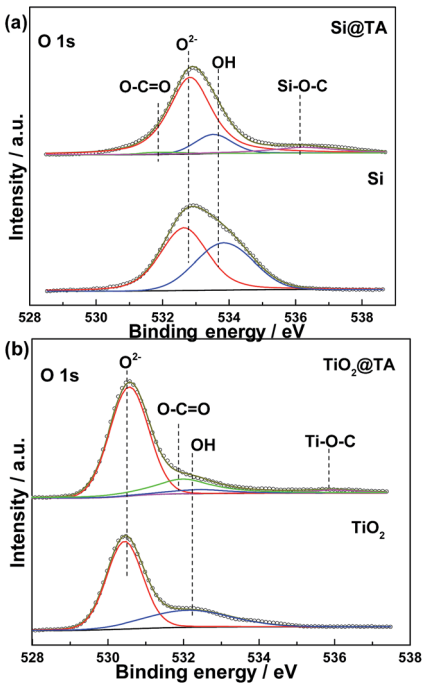

Fig. 3 XPS spectra of O 1s for (a) Si and Si@TA samples, and (b) TiO_2 and TiO_2@TA samples.

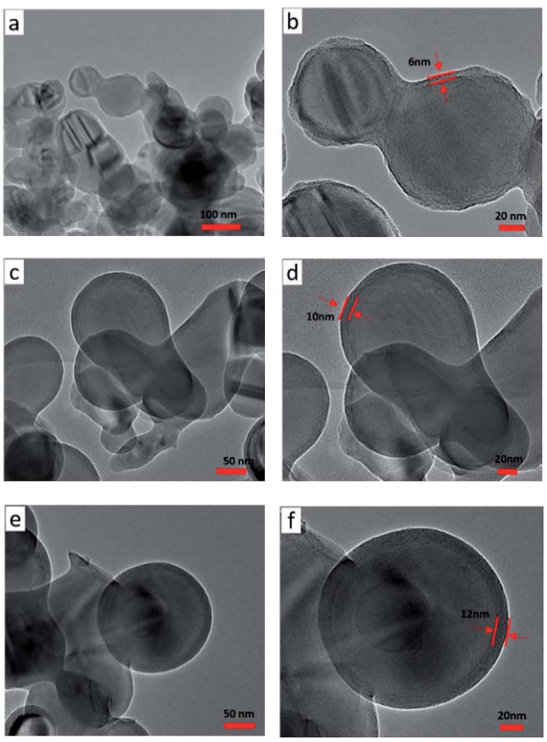

Fig. 4 TEM images of Si@C nanocomposites polymerized for (a) and (b) 6 h, (c) and (d) 12 h, and (e) and (f) 24 h.

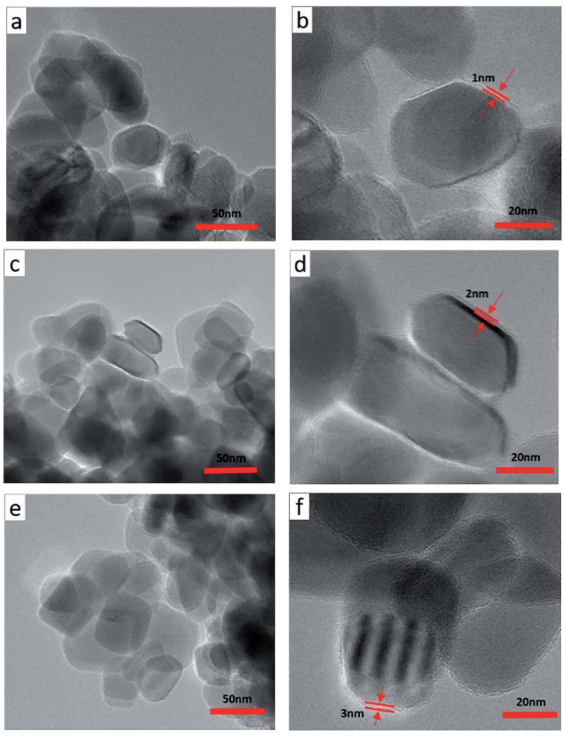

Fig. 5 TEM images of TiO_2@C nanocomposites for (a) and (b) 6 h, (c) and (d) 12 h, (e) and (f) 24 h.

The thickness of carbon shell directly affects the electrochemical performance of both Si and TiO_2 nanoparticles in the LIBs. When the carbon shell is too thin, it cannot restrict volume expansion during the charge–discharge process (for Si nanoparticles) and it is difficult to suppress the nano-sized cores clustering and limit excessive particle growth. When the carbon shell is too thick, however, it restricts the efficient ion transfer/transport. Therefore, it is important to obtain a carbon

shell with an optimized thickness. In our experiments, the carbon shell thickness on the pristine Si and TiO_2 nanoparticles will be controlled by the coating time. Fig. 4 and 5 show the Si@C and TiO_2@C nanocomposites with different coating times. It can be found that uniform and continuous carbon layers were coated on the surfaces of both Si and TiO_2 nanoparticles. Since the Si commercial nanoparticles have some native oxides on the surface, we treated the Si@C nanocomposites in an HF aqueous solution to remove these native oxides. By varying the coating times, Si@C nanocomposites with different thicknesses of carbon shell were prepared: ~6 nm for 6 h (Si@C-1), ~10 nm for 12 h (Si@C-2) and ~12 nm for 24 h (Si@C-3). The carbon contents, determined by thermogravimetric analysis (TGA-DTA), were about 7.6 wt% (Si@C-1), 10.8 wt% (Si@C-2) and 15.1 wt% (Si@C-3). For the TiO_2@C nanocomposites, the thicknesses of carbon shells and carbon contents were ~1 nm and 1.1 wt% for 6 h (TiO_2@C-1), ~2 nm and 1.9 wt% for 12 h (TiO_2@C-2) and ~3 nm and 3.0 wt% for 24 h (TiO_2@C-3) (Fig. 6).

Currently, the wide application of Si as an anode in LIBs is still impeded by the large volume expansion (up to 4 times) during the lithiation and delithiation which not only causes the pulverization of the electrode materials, but also leads to the delamination of the interface between the electrode material and the current collector, ultimately resulting in poor conductivity, cycling stability and rate capability of the batteries.[3,31] To restrict the volume expansion of Si and maintain the structural integrity, a uniform and continuous carbon layer with a thickness of 6–12 nm was coated onto the Si nanoparticles. We used the *in situ* TEM technique to observe the deformation and structural changes of the Si@C nanocomposites during the lithiation/delithiation processes. Fig. 7a shows the TEM images of the nano lithium-ion battery used for *in situ* lithiation/delithiation tests. Fig. 7b–d shows a series of images taken from a movie of the *in situ* lithiation/delithiation tests for the Si@C nanocomposites (ESI, Movie S1†). In Fig. 7b (0 s, before lithiation), the Si nanoparticle is visible within a surrounding carbon shell and there is a very small void space, caused by the removal of the native oxides, which is not big enough to accommodate the expansion in volume of the Si nanoparticle between the Si core and the carbon shell. The Si nanoparticle expands in volume as Li diffuses through the carbon layer and alloys with Si. The small void space between the core and shell disappeared after 11 s, which demonstrates that the Si nanoparticle is partially lithiated (discharging). After 44 s, the volume of the Si nanoparticle changes little, as seen from the TEM images, indicating that full lithiation is reached and no fracture of the carbon shell is observed after the lithiation of the Si nanoparticle. Fig. 7c shows the microstructure evolution during the delithiation (charging) of the Si@C nanocomposite. The gradual expansion of the space between the Si core and carbon shell shows the shrinkage of the Si nanoparticle as it is

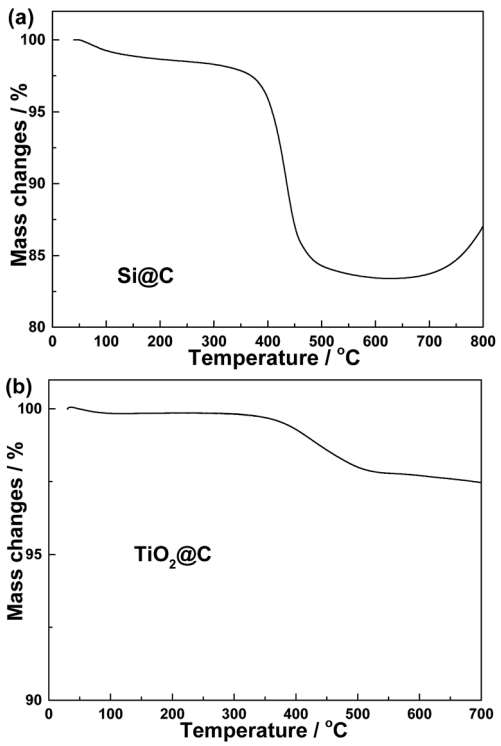

Fig. 6 Typical TG curves of (a) Si@C (24 h) and (b) TiO_2@C (24 h) nanocomposites.

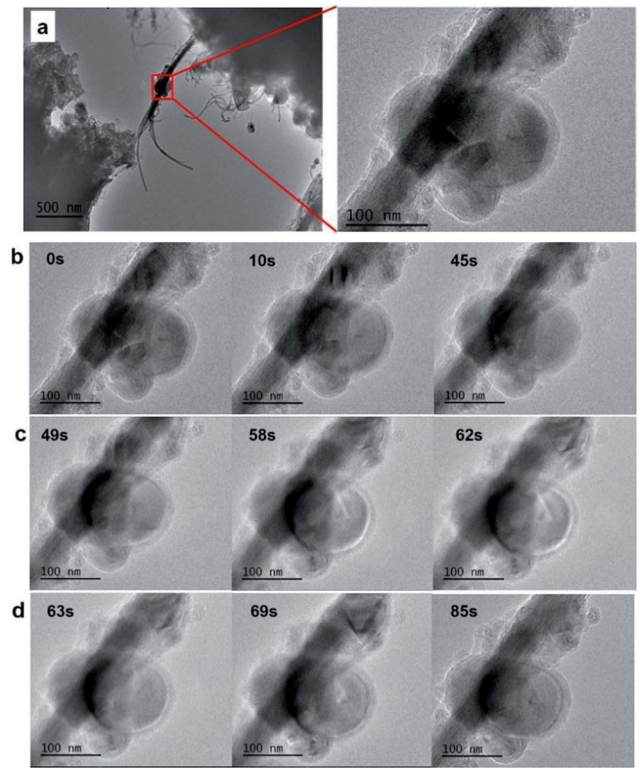

Fig. 7 (a) TEM image of the all-solid-state nano battery used for *in situ* lithiation/delithiation tests of the Si@C nanocomposites, where Li act as anode, Li_2O as electrolyte and a carbon-coated Si nanoparticle adhering to a CNT as cathode. *In situ* TEM images of the microstructure evolution of the Si@C nanoparticle during (b) the lithiation, (c) delithiation and (d) relithiation. All the TEM images are taken from Movie S1 in the ESI.† Note that the carbon shell did not rupture during the lithiation and delithiation processes.

being charged. Fig. 7d shows the microstructure evolution of the Si@C nanocomposite during the relithiation (redischarging), and also we cannot observe any fracture of the carbon shell. These results indicate that the carbon shell is so robust that it can protect and accommodate large volume expansion of the Si nanoparticle during the lithiation, effectively preventing the battery anode from changing structurally upon cycling.

The first three cycles of CV curves of both pristine Si and Si@C nanocomposites are shown in Fig. 8 within a potential range of 0.005–1.5 V at a scan rate of 0.2 mV s^{-1}. Both electrodes show typically Si-based cathodic and anodic peaks: the cathodic peaks at 0–0.4 V are attributable to the formation of Li_xSi alloys, and the corresponding anodic peaks at around 0.37 V and 0.55 V are related to the delithiation process of Li–Si alloys.[17,32] It is also observed that the intensity of anodic peaks for both electrodes enhanced in the first three cycles, which maybe due to the activation processes of Si electrodes.[17]

The cycling stability and specific capacity of LIBs will be directly affected by the carbon layer thickness of the Si@C nanocomposite. If the carbon layer is too thin, it is hard to protect and accommodate large volume expansion of Si cores during charging–discharging processes. To investigate the optimal thickness of carbon layers in the Si@C nanocomposites as anodes in the LIBs, we prepared Si@C nanocomposites with different thicknesses of carbon layers. Since the carbon layer is also lithiated as observed in the *in situ* TEM experiments (see Movie S1 in the ESI†), both the carbon shell and Si/TiO_2 core are contributing to the specific capacity. Therefore, the specific capacity values reported in our experiments are calculated on the basis of the total weight of both Si@C and TiO_2@C nanocomposites. The cycling performance of the pristine Si and all Si@C anodes in the LIBs are shown in Fig. 9a. For the cycling test, the cell was cycled at a rate of 0.1 A g^{-1} for one cycle, then 0.5 A g^{-1} for 3 cycles and 1 A g^{-1} for the later cycles. It was found that the specific capacity of the pristine Si anode rapidly decreased to less than 500 mA h g^{-1} after 10 cycles due to the large volume expansion of Si during the lithiation and delithiation. Thanks to the protective effect from the carbon shells, all Si@C nanocomposites show much better cycling stability than that of the pristine Si anode. After 200 cycles, the specific capacity of all Si@C anodes is above 700 mA h g^{-1}. The Si@C-3 anode (which declined from 1121.6 mA h g^{-1} to 1019.1 mA h g^{-1} after 200 cycles at 1 A g^{-1}) shows the highest cycling performance, higher than both Si@C-1 (declining from 1219.4 mA h g^{-1} to 764.2 mA h g^{-1} after 200 cycles at 1 A g^{-1}) and Si@C-2 (declining from 1180.4 mA h g^{-1} to 844.5 mA h g^{-1} after 200 cycles at 1 A g^{-1}) anodes due to the different thicknesses of carbon shells in the Si@C nanocomposites. Nyquist plots obtained from EIS measurements of all the pristine Si and Si@C electrodes are shown in Fig. 9b, and the equivalent circuit for this cell system is depicted, in which R_s is ohmic resistance of the electrolyte and cell components, R_{ct} is the charge transfer resistance, CPE is a constant phase element and W_f is the Warburg impedance.[32,33] The semicircular arc at the high-frequency region is related to the R_{ct} value. According to the fitted results, the values of charge transfer resistance for Si, Si@C-1, Si@C-2 and Si@C-3 anodes are 276.3 Ω, 204.2 Ω, 127.6 Ω and 91.2 Ω, respectively, and Si@C-3 shows the lowest transfer resistance value among all anode materials, indicating the best electron/ion transfer kinetics of the Si@C-3 anode with

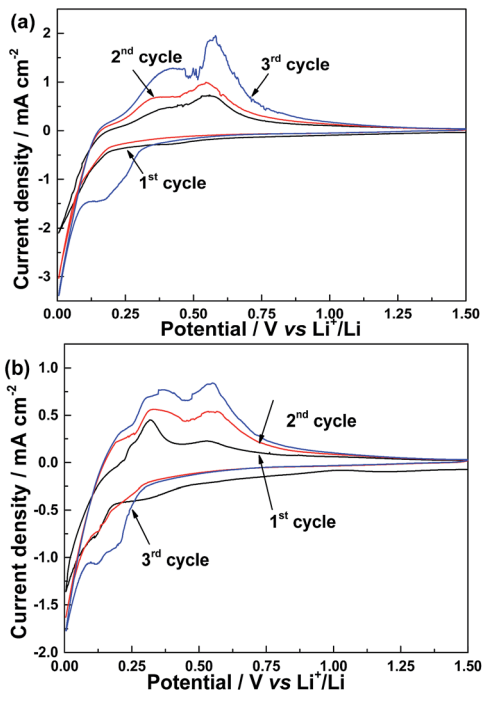

Fig. 8 Cyclic voltammogram curves of pristine (a) Si and (b) Si@C at a scan rate of 0.2 mV s^{-1} and at room temperature.

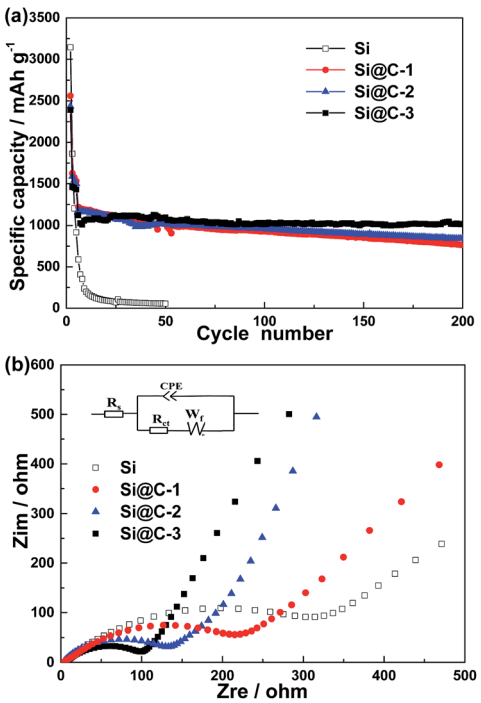

Fig. 9 (a) Discharge capacity *versus* cycle number plots of Si and Si@C nanocomposites. The rate was 0.1 A g^{-1} for one cycle, then 0.5 A g^{-1} for 3 cycles and 1 A g^{-1} for the later cycles. (b) Nyquist plots of Si and Si@C electrodes.

respect to the lithiation/delithiation process, which will be favorable for the electrochemical performance of a lithium-ion battery.

Since the Si@C-3 nanocomposites show good cycling stability and electron/ion transfer kinetic properties among all the Si@C nanocomposites, we systematically studied the electrochemical performance of the Si@C-3 nanocomposites in the LIBs, including their long-term cycle stability and rate capability. As shown in Fig. 10a, there is no clear capacity decay observed in the first 300 cycles, and the capacity retention value after 500 cycles was about 93.1% (~1000 mA h g^{-1}). The voltage profiles for the different cycles are shown in Fig. 10b. The shape of the profile does not change from the 25th to 500th cycle, indicating the stable electrochemical behavior of the Si@C nanocomposites. The Si@C core–shell structure is still well preserved after 500 cycles, as shown in the TEM image in Fig. 10c. In addition, the battery using the Si@C-3 nanocomposite as anode also showed good rate capability (Fig. 10d). Even at a rate of 10 A g^{-1}, the Si@C electrode can still show a specific capacity of 580 mA h g^{-1}, which is much higher than that of the theoretical specific capacity of graphite. Several current literatures have reported that the core–shell structure of Si@C nanocomposites improves the performance of Si-based anodes in lithium-ion batteries. For example, Ji *et al.* prepared NG/Si@NC composite, which exhibited an initial reversible capacity of 1142 mA h g^{-1} at a current density of 500 mA g^{-1} and remained at 938 mA h g^{-1} after 100 cycles with an 82% retention.[34] Li *et al.* prepared a core–shell structured graphite/silicon@pyrolyzed-carbon (G/Si@C) composite which showed a reversible capacity of 637.7 mA h g^{-1} and capacity retention of 89.5% after 100 cycles.[35] Li *et al.*[36] prepared hollow core–shell structured porous Si–C nanocomposites, which showed 650 mA h g^{-1} at 1 A g^{-1} after 100 cycles, and about 350 mA h g^{-1} at the rate of 8 A g^{-1}. Compared with the abovementioned researches, our Si@C electrode shows much better cycling performance and higher rate performance which is contributed by the uniform, continuous, robust and optimized thickness of carbon shell on the Si nanoparticles. Since the carbon layer is robust enough to restrain the large volume expansion of the Si anode, the SEI would not be ruptured during the charging–discharging processes.

The practical application of TiO_2 used as a typically safe anode material in LIBs is still hindered due to its low electronic conductivity, finally resulting in low specific capacity and poor cycling performance of batteries.[37,38] To solve this problem, a uniform and continuous carbon layer with about 1–3 nm was coated on the surface of the TiO_2 nanoparticles. TiO_2@C nanocomposites with different thicknesses of carbon layer can be obtained by varying the polymerization time: 6 h for TiO_2@C-1 (~1 nm), 12 h for TiO_2@C-2 (~2 nm) and 24 h for TiO_2@C-3 (~3 nm) (Fig. 5). The electronic conductivity improved because the carbon was coated on the surface of TiO_2. The electronic conductivity of TiO_2, TiO_2@C-1, TiO_2@C-2 and TiO_2@C-3 was 2.66×10^{-5} S cm^{-1}, 9.56×10^{-5} S cm^{-1}, 9.13×10^{-5} S cm^{-1} and 1.34×10^{-4} S cm^{-1}, respectively.

Cyclic voltammograms of both the pristine TiO_2 and TiO_2@C for the first three cycles at a rate of 0.2 mV s^{-1} within a potential

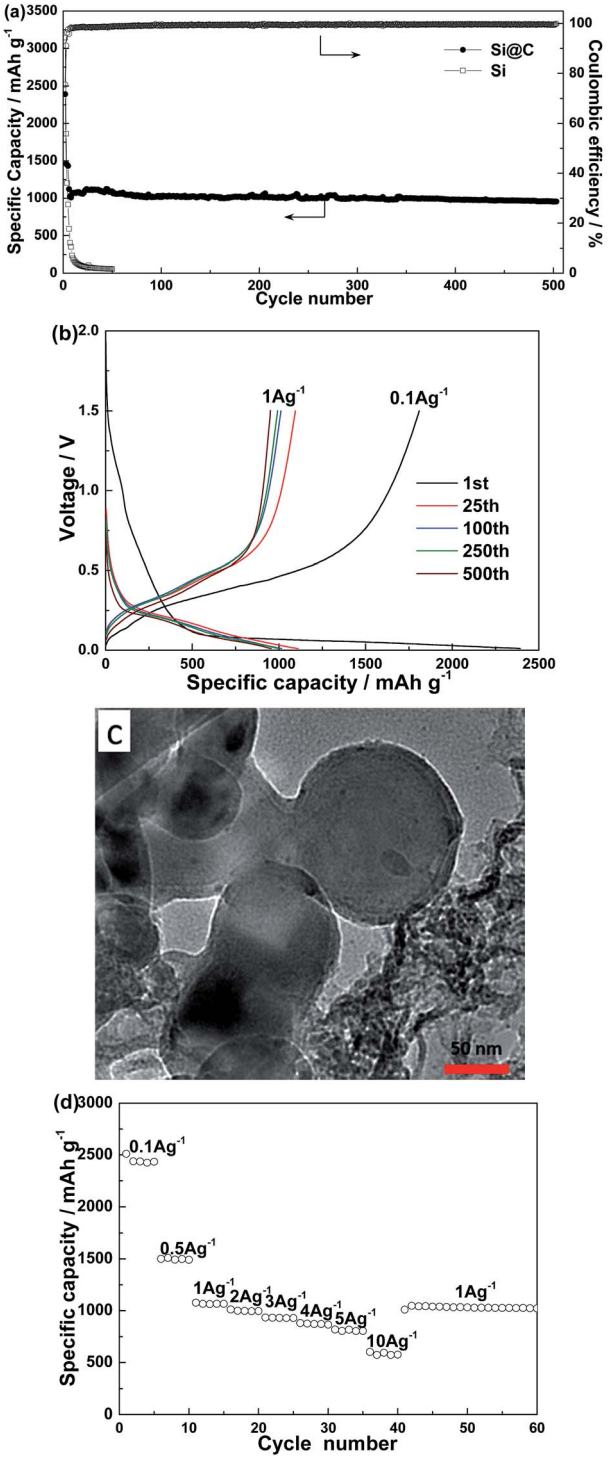

Fig. 10 Electrochemical performance of Si@C electrode in lithium-ion battery. (a) Discharge-capacity and CE *versus* cycle number plots of Si@C and Si nanoparticles as anodes. The rate was 0.1 A g^{-1} for one cycle, then 0.5 A g^{-1} for 3 cycles and 1 A g^{-1} for the later cycles. (b) Voltage profiles plotted for the first, 25th, 100th, 250th and 500th cycles. (c) TEM images of Si@C electrode after 500 cycles showing the Si@C core–shell structures still well resolved. (d) Rate capability of Si@C electrode.

range from 0.005 to 3.0 V are shown in Fig. 11. Two main current peaks are observed at about 1.75 V and 2.1 V during cathodic and anodic sweeps, which correspond to the lithiation and delithiation of Li_xTiO_2.[39,40] The peak at 0.6 V of TiO_2@C at the first lithiation process contributes to the formation of SEI. The oxidation peak at 2.35 V of TiO_2@C in the first cycle declined rapidly during the subsequent cycling process, which may be ascribed to irreversible oxidation of the electrolyte or organic impurities.[38]

The electrochemical performance of the TiO_2@C nanocomposite was improved (Fig. 12). The voltage profiles of the first cycle at C/10 rate of the electrodes based on TiO_2 and TiO_2@C nanocomposite are shown in Fig. 12a. Both the electrodes show the characteristic features of anatase TiO_2 upon lithiation (discharge) and subsequent delithiation (charge). The performance of the first cycle of the battery with the TiO_2@C anode (charge capacity: 233.1 mA h g^{-1}, discharge capacity: 253.3 mA h g^{-1}, coulombic efficiency: 92.0%) was better than that of the battery with the pristine TiO_2 anode (charge capacity: 187.7 mA h g^{-1}, discharge capacity: 222.9 mA h g^{-1}, coulombic efficiency: 84.2%). Fig. 12b shows the cycling performance of the pristine TiO_2 and all TiO_2@C anodes at a current density of 0.5C between 1.0 and 3.0 V. It can be found that the electrochemical performance of the TiO_2@C electrode was better than that of the pristine TiO_2 electrode. The first cycle discharge capacities of the pristine TiO_2, TiO_2@C-1, TiO_2@C-2 and TiO_2@C-3 electrodes were about 147.5 mA h g^{-1}, 162.3 mA h g^{-1},165.6 mA h g^{-1} and 167.4 mA h g^{-1}, respectively. It can be found that the capacity of the TiO_2@C electrode was higher

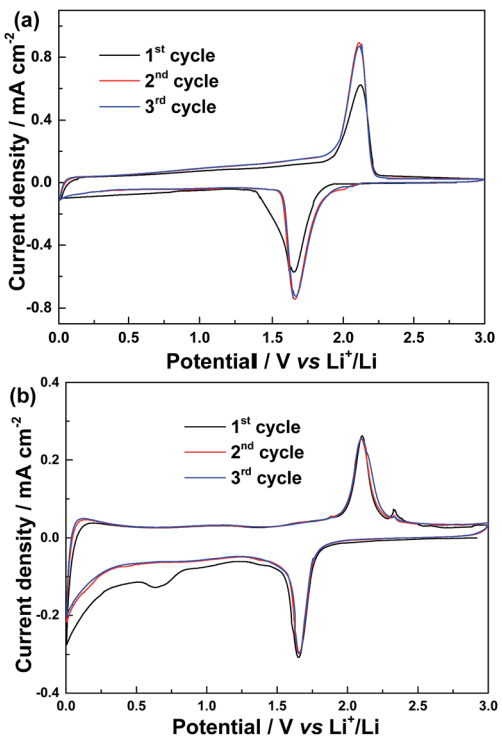

Fig. 11 Cyclic voltammogram curves of pristine (a) TiO_2 and (b) TiO_2@C at a scan rate of 0.2 mV s^{-1} and at room temperature.

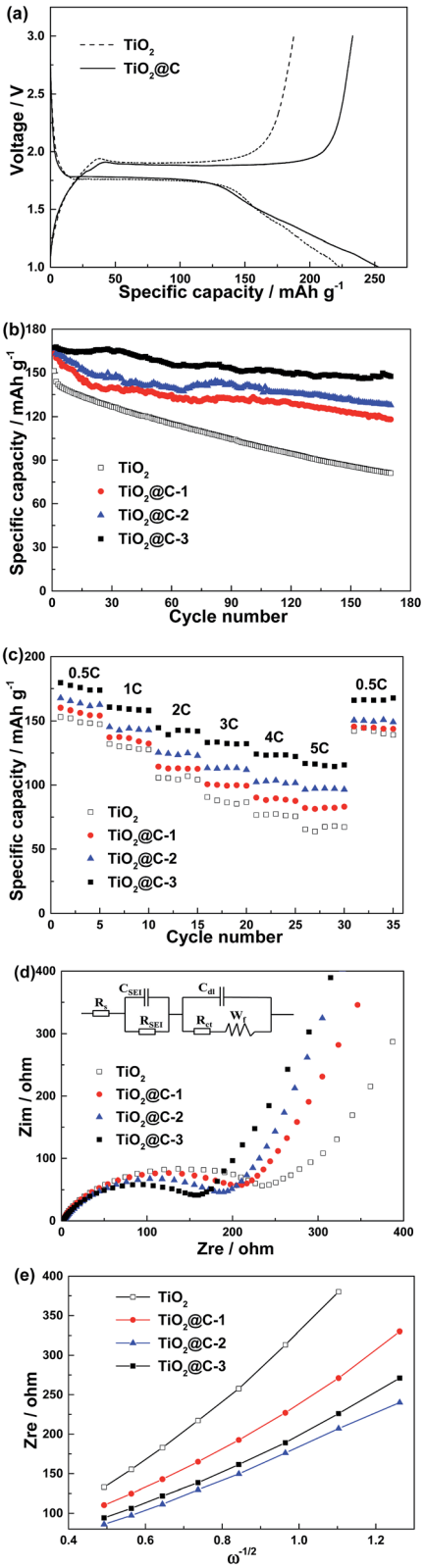

Fig. 12 Electrochemical performance of TiO_2@C electrode in lithium-ion battery. (a) Voltage profiles of TiO_2 and TiO_2@C electrodes during the first cycle at 0.1C. (b) Discharge capacity *versus* cycle number plots of TiO_2 and TiO_2@C electrodes. Rate: 0.5C. (c) Rate capability of TiO_2 and TiO_2@C electrodes. (d) and (e) Nyquist plots of TiO_2 and TiO_2@C electrodes after 170th cycle at 0.5C.

than that of the pristine TiO_2 electrode due to the carbon coated onto the TiO_2 nanoparticles. The cycling performance of the pristine TiO_2 electrode was very poor and the capacity declined to about 81.1 mA h g^{-1} (53.6% of the first cycle capacity) after the 170th cycle. In contrast, the TiO_2@C electrode showed excellent cycling stability. After 170 cycles, the capacity loss was about 27.2% (about 118.1 mA h g^{-1}), 22.8% (about 127.9 mA h g^{-1}) and 11.9% (about 147.5 mA h g^{-1}) for TiO_2@C-1, TiO_2@C-2 and TiO_2@C-3 electrodes, respectively. In addition, the TiO_2@C electrode showed higher rate capability than that of the pristine TiO_2 electrode at different rates, as shown in Fig. 12c. It can be found that the TiO_2@C-3 anode with about a 3 nm thick carbon shell shows the best cycling stability, highest specific capacity and best rate capability among all the TiO_2@C nanocomposites.

Due to the presence of the uniform carbon coating layer, the TiO_2@C electrode exhibited lower resistance than that of the pristine TiO_2 electrode as shown by the reduced diameter of the semicircle at the high-frequency region and the appreciably steep slope line at the low-frequency region in the electrochemical impedance spectroscopy (EIS) (Fig. 12d). Nyquist plots obtained from EIS measurements of the pristine TiO_2 and TiO_2@C electrodes after 170 cycles are shown in Fig. 12d and e. The values of charge transfer resistance (R_{ct}) for TiO_2, TiO_2@C-1, TiO_2@C-2 and TiO_2@C-3 are 230.5 Ω, 187.6 Ω, 179.1 Ω, and 130.7 Ω, respectively. The R_{ct} values of all TiO_2@C nanocomposites are smaller than that of the pristine TiO_2. The value of R_{ct} was in the order: TiO_2@C-3 < TiO_2@C-2 < TiO_2@C-1 < TiO_2. The diffusion coefficient D of the lithium ion can be calculated from plots in the low-frequency region according to the following equation:[39]

$$D = R^2T^2/2A^2n^4F^4C^2\sigma^2 \quad (1)$$

σ is the Warburg factor which has the relationship with Z_{re} as follows:[41]

$$Z_{re} = R_{ct} + R_s + \sigma\omega^{-1/2} \quad (2)$$

Based on eqn (1) and (2), the values of the diffusion coefficients of TiO_2, TiO_2@C-1, TiO_2@C-2 and TiO_2@C-3 are 5×10^{-13} cm^2 s^{-1}, 1.07×10^{-12} cm^2 s^{-1}, 1.45×10^{-12} cm^2 s^{-1} and 1.27×10^{-12} cm^2 s^{-1}, respectively. Compared with the pristine TiO_2, the TiO_2@C nanocomposites show a higher Li^+ ion diffusion ability. The value of the diffusion coefficient of Li^+ ion was in the order: TiO_2@C-2 > TiO_2@C-3 > TiO_2@C-1 > TiO_2. The results of the EIS confirm the improvement of the electronic conductivity and ion permeability of the carbon shell, which will be favorable for the electrochemical performance of the lithium-ion battery during cycling. Among all TiO_2@C nanocomposites, the TiO_2@C-3 shows the best cycling performance, which was also confirmed by the EIS result. Although the value of diffusion coefficient of TiO_2@C-3 is a little lower than that of TiO_2@C-2, the lower R_{ct} and the thicker carbon layer that can suppress the volume change, which finally results in making the TiO_2@C-3 electrode have the better cycling performance.

Conclusions

In conclusion, we developed a versatile and cheap method to synthesize core–shell carbon nanocomposites using tannic acid as the carbon source. The uniform and continuous carbon layers with a controlled thickness on the surface of the Si and TiO_2 nanoparticles were obtained easily by a simple immersion of both nanoparticles in a tannic acid aqueous solution and subsequent carbonization. Due to the carbon shells, both Si@C and TiO_2@C nanocomposites used as anode materials in lithium-ion batteries showed excellent electrochemical performance, such as higher specific capacity, better cycling stability and higher rate capability. We expect that this coating method may be utilized in the construction of various nano-structured carbon-based materials, such as core–shell, yolk–shell, rattle-type, and hollow carbon nanospheres or capsules.

Acknowledgements

This research was supported by Natural Science Foundation of Shanghai (14ZR1422100), Science and Technology Commission of Shanghai Municipality (14DZ2250800). Thanks to the Instrumental Analysis Center of Shanghai Jiaotong University.

Notes and references

1 F. Caruso, *Adv. Mater.*, 2001, **13**, 11.
2 Y. Wang, A. S. Angelatos and F. Caruso, *Chem. Mater.*, 2007, **20**, 848.
3 L. Su, Y. Jing and Z. Zhou, *Nanoscale*, 2011, **3**, 3967.
4 L. Luo, H. Yang, P. Yan, J. J. Travis, Y. Lee, N. Liu, D. M. Piper, S.-H. Lee, P. Zhao, S. M. George, J.-G. Zhang, Y. Cui, S. Zhang, C. Ban and C.-M. Wang, *ACS Nano*, 2015, **9**, 5559.
5 Y. Zhang, L. Jiang and C. Wang, *Nanoscale*, 2015, **7**, 11940.
6 S. L. Yang, B. H. Zhou, M. Lei, L. P. Huang, J. Pan, W. Wu and H. B. Zhang, *Chin. Chem. Lett.*, 2015, **26**, 1293.
7 H. Zhang, Y. Dai, H. Zhang, W. Wang, Q. Huang, Y. Chen and L. Pu, *Int. J. Electrochem. Sci.*, 2016, **11**, 6279.
8 S. M. Abbas, S. T. Hussain, S. Ali, N. Ahmad, N. Ali and K. S. Munawar, *Electrochim. Acta*, 2013, **105**, 481.
9 S. W. Oh, S. T. Myung, S. M. Oh, K. H. Oh, K. Amine, B. Scrosati and Y. K. Sun, *Adv. Mater.*, 2010, **22**, 4842.
10 L. Tan, L. Pan, C. Cao, B. Wang and L. Li, *J. Power Sources*, 2014, **253**, 193.
11 Y. N. Jo, Y. Kim, J. S. Kim, J. H. Song, K. J. Kim, C. Y. Kwag, D. J. Lee, C. W. Park and Y. J. Kim, *J. Power Sources*, 2010, **195**, 6031.
12 S. J. Park, Y. J. Kim and H. Lee, *J. Power Sources*, 2011, **196**, 5133.
13 X. Y. Zhang, H. P. Li, X. L. Cui and Y. Lin, *J. Mater. Chem.*, 2010, **20**, 2801.
14 K. S. Raja, M. Misra, V. K. Mahajan, T. Gandhi, P. Pillai and S. K. Mohapatra, *J. Power Sources*, 2006, **161**, 1450.
15 K. Xie, P. Wu, Y. Zhou, Y. Ye, H. Wang, Y. Tang and T. Lu, *ACS Appl. Mater. Interfaces*, 2014, **6**, 10602.
16 P. Wu, N. Du, H. Zhang, J. Yu, Y. Qi and D. Yang, *Nanoscale*, 2011, **3**, 746.

17 H. Wang, P. Wu, H. Shi, F. Lou, Y. Tang, T. Zhou and T. Lu, *Mater. Res. Bull.*, 2014, **55**, 71.
18 A. H. Lu, T. Sun, W. C. Li, Q. Sun, F. Han, D. H. Liu and Y. Guo, *Angew. Chem., Int. Ed.*, 2011, **50**, 6799.
19 T. S. Sileika, D. G. Barrett, R. Zhang, K. H. A. Lau and P. B. Messersmith, *Angew. Chem., Int. Ed.*, 2013, **52**, 10766.
20 L. Pan, H. Wang, C. Wu, C. Liao and L. Li, *ACS Appl. Mater. Interfaces*, 2015, **7**, 16003.
21 S. L. Cumberland and G. F. Strouse, *Langmuir*, 2002, **18**, 269.
22 S. S. Shankar, A. Rai, A. Ahmad and M. Sastry, *J. Colloid Interface Sci.*, 2004, **275**, 496–502.
23 D. S. Sheny, J. Mathew and D. Philip, *Spectrochim. Acta, Part A*, 2011, **79**, 254.
24 D. Philip and C. Unni, *Phys. E*, 2011, **43**, 1318.
25 H. Lee, N. F. Scherer and P. B. Messersmith, *Proc. Natl. Acad. Sci. U. S. A.*, 2006, **103**, 12999.
26 E. McCafferty and J. P. Wightman, *Surf. Interface Anal.*, 1998, **26**, 549.
27 B. Erdem, R. A. Hunsicker, G. W. Simmons, E. D. Sudol, V. L. Dimonie and M. S. El-Aasser, *Langmuir*, 2001, **17**, 2664.
28 X. M. Wu, L. L. Wang, Y. Wang, J. S. Gu and H. Y. Yu, *J. Membr. Sci.*, 2012, **421**, 60.
29 R. Rodríguez, M. A. Blesa and A. E. Regazzoni, *J. Colloid Interface Sci.*, 1996, **177**, 122.
30 J. L. Dalsin, L. Lin, S. Tosatti, J. Vörös and M. Textor, *Langmuir*, 2005, **21**, 640.
31 M. L. Terranova, S. Orlanducci, E. Tamburri, V. Guglielmotti and M. Rossi, *J. Power Sources*, 2014, **246**, 167.
32 W. Li, Y. Tang, W. Kang, Z. Zhang, X. Yang, Y. Zhu and C. S. Lee, *Small*, 2015, **11**, 1345.
33 S. Yang, X. Feng, L. Zhi, Q. Cao, J. Maier and K. Müllen, *Adv. Mater.*, 2010, **22**, 838.
34 D. Ji, Y. Wan, Z. Yang, C. Li, G. Xiong, L. Li and H. Luo, *Electrochim. Acta*, 2016, **192**, 22.
35 J. Li, J. Wang, J. Yang, X. Ma and S. Lu, *J. Alloys Compd.*, 2016, **688**, 1072.
36 X. Li, P. Meduri, X. Chen, W. Qi, M. H. Engelhard, W. Xu and J. G. Zhang, *J. Mater. Chem.*, 2012, **2**, 11014.
37 G. N. Zhu, Y. G. Wang and Y. Y. Xia, *Energy Environ. Sci.*, 2012, **5**, 6652.
38 Z. Yang, D. Choi, S. Kerisit, K. M. Rosso, D. Wang, J. Zhang, G. Graff and J. Liu, *J. Power Sources*, 2009, **192**, 588.
39 J. Wang, L. Shen, H. Li, X. Wang, P. Nie, B. Ding and X. Zhang, *Electrochim. Acta*, 2014, **133**, 209.
40 Y. Chen, X. Ma, X. Cui and Z. Jiang, *J. Power Sources*, 2016, **302**, 233.
41 Q. Cao, H. P. Zhang, G. J. Wang, Q. Xia, Y. P. Wu and H. Q. Wu, *Electrochem. Commun.*, 2007, **9**, 1228.

